



# Hydrodeoxygenation of m-cresol over nickel and nickel phosphide based catalysts. Influence of the nature of the active phase and the support



Vinicio O.O. Gonçalves<sup>a</sup>, Priscilla M. de Souza<sup>b</sup>, Thierry Cabioc'h<sup>c</sup>,  
Victor Teixeira da Silva<sup>b</sup>, Fabio B. Noronha<sup>d,e</sup>, Frédéric Richard<sup>a,\*</sup>

<sup>a</sup> Institut de Chimie des Milieux et Matériaux de Poitiers, UMR 7285 Université de Poitiers – CNRS, 4, rue Michel Brunet, BP633, 86022 Poitiers Cedex, France

<sup>b</sup> Universidade Federal do Rio de Janeiro, Chemical Engineering Program – COPPE, Caixa Postal 68502, CEP 21941-972, Rio de Janeiro, RJ, Brazil

<sup>c</sup> Institut Pprime, UPR 3346 CNRS – Université de Poitiers – ISAE-ENSMA, BP 30179, 86962 Futuroscope-Chasseneuil Cedex, France

<sup>d</sup> Catalysis Division, National Institute of Technology, Av. Venezuela 82, 20081-312, Rio de Janeiro, 20081-312, Brazil

<sup>e</sup> Chemical Engineering Department, Military Institute of Engineering, Praça Gal. Tibúrcio 80, 22290-270, Rio de Janeiro, Brazil

## ARTICLE INFO

### Article history:

Received 26 April 2017

Received in revised form 12 July 2017

Accepted 15 July 2017

Available online 21 July 2017

### Keywords:

m-cresol

Nickel catalyst

HDO

Nickel phosphide catalyst

Effect of support

## ABSTRACT

The present work studied the effect of two supports ( $\text{SiO}_2$  and tetragonal  $\text{ZrO}_2$ ) on the performance of metallic nickel and nickel phosphide catalysts for the hydrodeoxygenation (HDO) of m-cresol carried out at 340 °C under 4 MPa. All catalysts were characterized using several techniques (ICP,  $\text{N}_2$  adsorption-desorption, XRD,  $\text{H}_2$ -TPR,  $\text{NH}_3$ -TPD). The active phases ( $\text{Ni}(0)$  and  $\text{Ni}_2\text{P}$ ) were successively prepared at 450 °C under 4 MPa of  $\text{H}_2$ , as observed by XRD. The activity and deoxygenation properties depended on the active phase (Ni vs  $\text{Ni}_2\text{P}$ ) and the support ( $\text{SiO}_2$  vs  $\text{ZrO}_2$ ). The order of HDO activity ( $\text{mmol g}^{-1} \text{h}^{-1}$ ) followed:  $\text{Ni}_2\text{P}/\text{ZrO}_2$  (47.0) >  $\text{Ni}_2\text{P}/\text{SiO}_2$  (28.3) »  $\text{Ni}/\text{ZrO}_2$  (3.0) >  $\text{Ni}/\text{SiO}_2$  (1.1). The  $\text{Ni}_2\text{P}$  phase was clearly much more active than metallic Ni. In addition, the use of zirconia as support enhanced the deoxygenation properties compared to silica, which can be attributed to the presence of oxophilic sites ( $\text{Zr}^{3+}/\text{Zr}^{4+}$ ) favoring the adsorption of m-cresol.

© 2017 Elsevier B.V. All rights reserved.

## 1. Introduction

Hydrodeoxygenation (HDO) is an important process to upgrade pyrolysis bio-oil to produce suitable biofuels or blendings to be add into existing fuels [1–4]. Most of the undesired properties of bio-oil (chemical instability, corrosivity, acidity, low heating value, high viscosity and immiscibility with conventional fuels) can be eliminated by oxygen removal by reacting its oxygenated molecules with  $\text{H}_2$  using a specific catalyst [5,6].

In the research of an appropriate catalyst for the HDO process, metal sulfides catalysts, conventionally used in petroleum refining (e.g.,  $\text{NiMoS}$  and  $\text{CoMoS}$ ), were the first catalysts tested in such reaction. Although sulfides catalysts are active for HDO with a high selectivity to deoxygenated products [7,8], their main disadvantage is the need for sulfur addition to the feed to maintain the catalytic activity, which can eventually lead to the formation of sulfur compounds [9,10].

Noble metal catalysts also exhibit high activity toward deoxygenation products [11–13], but they are very expensive, which limits their commercial application. The non-noble metal catalysts are more cost effective than noble metal catalysts and show acceptable catalytic performance [14,15]. In particular, Ni-based catalysts have been extensively studied for hydrodeoxygenation of different bio-oil model compounds [14–22]. The improvement of HDO activity for Ni catalysts was observed with the use of oxophilic supports like zirconia [13,14,16,20,21]. For example,  $\text{Ni}/\text{ZrO}_2$  and  $\text{Pd}/\text{ZrO}_2$  catalysts were more selective to benzene than  $\text{Pd}/\text{SiO}_2$  and  $\text{Ni}/\text{SiO}_2$  for HDO of phenol at 300 °C under atmospheric pressure [13]. Mortensen et al. [14] also reported the best performance for  $\text{Ni}/\text{ZrO}_2$  among a series of catalysts ( $\text{Ni}/\text{Al}_2\text{O}_3$ ,  $\text{Ni}/\text{SiO}_2$ ,  $\text{Ni}/\text{MgAl}_2\text{O}_4$ ,  $\text{Ni}/\text{CeO}_2/\text{ZrO}_2$ ,  $\text{Ni}/\text{CeO}_2$ ,  $\text{Ni}/\text{C}$ ,  $\text{Ru}/\text{C}$  and  $\text{Pd}/\text{C}$ ) for the deoxygenation of phenol (275 °C, 10 MPa). In summary, the striking difference in selectivity toward deoxygenated products for these catalysts could be related to the adsorption mode of oxygenated compounds. On  $\text{Ni}/\text{ZrO}_2$ , the HDO activity was facilitated by preferential interaction between Zr cations (oxophilic sites) and the oxygen atom of a model molecule, as confirmed by Foraita et al. [21].

\* Corresponding author.

E-mail address: [frédéric.richard@univ-poitiers.fr](mailto:frédéric.richard@univ-poitiers.fr) (F. Richard).

Recently, transition metal phosphides ( $M_xP_y$ ) have been studied for HDO reactions of different representative model compounds of bio-oil [23–34]. There are several interesting features in the use of these active phases, they are more economical than noble metal catalysts and less susceptible to secondary reactions (hydrogenolysis of C–C bond and methanation) than non-noble metal catalysts. The high performance of transition metal phosphides has been attributed to the presence of phosphorous that provides “ligand” (or electronic) and “ensemble” (or geometrical) effects on metal sites [29,30]. Overall, phosphide catalysts show bifunctional properties (acid/metal function) and the presence of P species may lead to the formation of P-OH groups, increasing their acidity [31]. Among a series of metal phosphides ( $Ni_2P$ ,  $Co_2P$ ,  $Fe_2P$ , WP, MoP),  $Ni_2P$  revealed superior activity for deoxygenation and higher stability [23–25,28]. Infantes-Molina et al. [28] attributed the best performance of  $Ni_2P$  in the hydrodeoxygénéation of dibenzofuran to the higher amount of P-OH species on the catalyst, which can prevent the oxidation of  $Ni_2P$  phase and also act as H-donors (weak acid sites), hydrogenating C species on surface and reducing coke formation. Therefore, phosphide catalysts could present high stability in HDO of model molecules representative of bio-oil. However, water produced in the reaction may lead to catalyst deactivation depending on the type of the phosphide catalyst. Li et al. [23] observed that MoP/SiO<sub>2</sub> was more susceptible to oxidation and less active for HDO of anisole (300 °C, 1.5 MPa) than the  $Ni_2P$ /SiO<sub>2</sub> due to higher affinity of Mo with oxygen from water compared to Ni. Recently, our group also reported that  $Ni_2P$ /SiO<sub>2</sub> remained quite stable during the HDO of cresols isomers for at least 20 h of reaction using high pressure of H<sub>2</sub> [27]. In the same study, the product distribution was explained by the presence of different active sites on  $Ni_2P$  phase (Ni(1) and Ni(2)) and adsorption modes on the catalyst. Ni(1) sites present on the  $Ni_3P_2$  termination interact with the oxygen atom of C–OH bond and facilitate the hydrogenolysis reactions of cresols into toluene and methylcyclohexanols into methylcyclohexane whereas Ni(2) sites of  $Ni_3P$  termination promote a flat adsorption of cresols, favoring the hydrogenation of aromatic ring.

Although it is well known that the nature of support influences the product distribution and the extent of the HDO reaction, only a few studies investigated the effect of the type of support on the performance of phosphide catalysts in HDO of model molecules [26,32–34], which appears fairly complex. The type of support can affect the nature of phosphide phase formed and it may lead to the formation of phosphate species with the support upon calcination (like AlPO<sub>4</sub> when Al<sub>2</sub>O<sub>3</sub> is used as support) [26]. Moon and Lee [34] showed that the support can protect the  $Ni_2P$  phase against oxidation by water during the HDO of guaiacol (300 °C, 3 MPa). Indeed, under the employed conditions, the  $Ni_2P$ /SiO<sub>2</sub> catalyst was oxidized to nickel phosphate by water whereas the  $Ni_2P$  phase supported on zirconia and active carbon was resistant to oxidation. The order of activity determined over fresh catalysts was the following:  $Ni_2P$ /SiO<sub>2</sub> >  $Ni_2P$ /ZrO<sub>2</sub> >  $Ni_2P$ /AC (AC = active carbon), whereas using recycled catalysts, the order of activity became  $Ni_2P$ /ZrO<sub>2</sub> >  $Ni_2P$ /AC >  $Ni_2P$ /SiO<sub>2</sub>. Wu et al. [33] also investigated the HDO of guaiacol at the same temperature (300 °C) but under atmospheric pressure over the same nickel phosphide phase ( $Ni_2P$ ) supported on alumina, zirconia and silica. The intrinsic activity decreased in the following order:  $Ni_2P$ /ZrO<sub>2</sub> >  $Ni_2P$ /Al<sub>2</sub>O<sub>3</sub> >  $Ni_2P$ /SiO<sub>2</sub>. As a result, the order of activity between  $Ni_2P$ /SiO<sub>2</sub> and  $Ni_2P$ /ZrO<sub>2</sub> is still controversial.

Concerning the differences in HDO activity between Ni and  $Ni_2P$  phases, there are still some uncertainties in the literature. Indeed, it was reported that  $Ni$ /SiO<sub>2</sub> and  $Ni_2P$ /SiO<sub>2</sub> exhibited practically the same activity for the HDO of anisole (300 °C, 1.5 MPa) [23] and of methyl laurate (300 °C, 2 MPa) [35], whereas  $Ni$ /SiO<sub>2</sub> was found to be much more active than  $Ni_2P$ /SiO<sub>2</sub> for HDO of guaiacol (350 °C, 0.5 MPa) [36]. These differences in behavior could be explained by

both the nature of the oxygenated reactant and the experimental conditions used.

In order to clarify the effect of the active phase and the support, the present work investigated the effect use of SiO<sub>2</sub> and tetragonal ZrO<sub>2</sub> as supports for metallic nickel and nickel phosphide for HDO of m-cresol (340 °C, 4 MPa). The evaluation of the catalytic properties (activity, selectivity and stability) was performed and discussed. The use of a kinetic model also grounded the discussions.

## 2. Experimental

### 2.1. Catalyst synthesis

Silica (Hi-Sil 915, PPG Industries) and ZrO<sub>2</sub> (Saint-Gobain Nor-Pro) were used as supports. Prior to impregnation, silica was calcined under air flow at 800 °C for 5 h. No previous treatment was performed on zirconia. Ni/SiO<sub>2</sub> and Ni/ZrO<sub>2</sub> samples were prepared by incipient wetness impregnation of the supports (IWI method) using an aqueous solution of nickel nitrate hexahydrate ( $Ni(NO_3)_2 \cdot 6H_2O$ , Merck) to obtain 10 wt.% of Ni. Both solids were then dried under air flow (60 mL min<sup>-1</sup>) at 120 °C for 24 h and then calcined in air at 500 °C for 3 h (2 °C min<sup>-1</sup>). Nickel phosphide catalysts (NiP/SiO<sub>2</sub> and NiP/ZrO<sub>2</sub>) were also synthesized by IWI method to obtain the oxide precursors of the phosphide phase ( $Ni_xPyO_z$ ). In the first step, nickel nitrate hexahydrate ( $Ni(NO_3)_2 \cdot 6H_2O$ , Merck) and ammonium hydrogen phosphate ( $(NH_4)_2HPO_4$ , Vetec) salts were solubilized separately in distilled water. The solution of  $(NH_4)_2HPO_4$  was added dropwise to an aqueous solution containing  $Ni(NO_3)_2 \cdot H_2O$  under magnetic stirring and a precipitate was formed. Then, nitric acid (HNO<sub>3</sub>, Vetec) was added dropwise until complete solubilization of the precipitate. The concentration of the precursor solutions was adjusted to obtain catalysts with 10 wt.% of nickel. According to previous reports, an excess of phosphorus is required when an acid support was used [32]. Thus, the P/Ni molar ratio for  $Ni_2P$ /SiO<sub>2</sub> and  $Ni_2P$ /ZrO<sub>2</sub> catalysts was 0.8 and 3.0, respectively, in order to guarantee the formation of the  $Ni_2P$  phase. The resultant solution was impregnated onto both ZrO<sub>2</sub> and SiO<sub>2</sub> supports for Ni-based catalysts. Afterwards, these solids were also dried and calcined as previously described. Both nickel and phosphide phases were finally prepared after in situ treatment as further discussed. Prior to use, all catalysts were pelleted, crushed and sieved with 250–315 µm.

### 2.2. Catalyst characterization

The chemical composition of nickel oxide and the oxidic precursors of nickel phosphides over SiO<sub>2</sub> and ZrO<sub>2</sub> were determined by inductively coupled plasma optical emission spectrometry (ICP-OES) using an SPECTRO ARCOS ICP-OES instrument. Prior to analysis, the samples were digested with concentrated nitric acid and hydrofluoric acid using microwave heating system.

Textural properties of the solids were obtained using the N<sub>2</sub> adsorption–desorption isotherms acquired on a Micromeritics ASAP 2000 analyzer at –196 °C. Prior to N<sub>2</sub> adsorption, the solid samples were degassed overnight under secondary vacuum at 200 °C. The specific surface area ( $S_{BET}$  in m<sup>2</sup> g<sup>-1</sup>) was calculated from the adsorption isotherm (P/P<sub>0</sub> between 0.05 and 0.20) using the Brunauer–Emmett–Teller (B.E.T.) method. The total pore volume was calculated from the adsorbed volume of nitrogen at P/P<sub>0</sub> equal to 0.98. The mesoporous volume was determined using the t-plot method. The average mesopore-size distribution was calculated from the adsorption isotherm branch using the Barrett–Joyner–Halenda (BJH) method.

X-ray diffraction (XRD) diagrams were obtained using the Cu K $\alpha$  radiations in a Bruker D8 advance diffractometer in a Bragg–

Brentano geometry in the range 20–90° for 2q. The instrument was operated at 40 kV and 40 mA. Interval steps of 0.04° or 0.06° for 2θ and acquisition time varying between 10 and 20 s for each step were used with a LYNX EYE rapid detector. The pattern of a Cr<sub>2</sub>O<sub>3</sub> powder (Standard NIST 674b) was collected at the same geometrical conditions to generate an instrumental resolution function to account for the experimental broadening. Rietveld refinements of the diffractograms were performed using the Materials Analysis Using Diffraction (MAUD) software [37]. Prior to analysis, the catalysts were treated at 450 °C (5 °C min<sup>-1</sup>) under 4 MPa as total pressure during 2 h using pure hydrogen (4.7 NL h<sup>-1</sup>). After activation in situ, samples were cooled down under hydrogen to 25 °C and passivated at this temperature under atmospheric pressure for 3 h by a flow of 5 vol.% O<sub>2</sub> in He (80 mL min<sup>-1</sup>).

The reducibility of the supported oxide precursors of Ni and Ni<sub>x</sub>P<sub>y</sub>O<sub>z</sub> were characterized by the H<sub>2</sub> temperature-programmed reduction (H<sub>2</sub>-TPR) using a Micromeritics AutoChem 2910. Prior to analysis, each sample (100 mg) was pretreated under He flow (20 mL min<sup>-1</sup>) at 200 °C (heating rate of 10 °C min<sup>-1</sup>) for 30 min. Then, the catalyst was cooled down to 50 °C. The measurements started at this temperature using 10% H<sub>2</sub> in Ar (20 mL min<sup>-1</sup>). The temperature was progressively increased until 1000 °C (heating rate of 5 °C min<sup>-1</sup>) and held for 90 min. The hydrogen consumption was estimated using a TCD detector. The reduction into phosphide catalysts was also carried out in a system coupled to a VC 40 Thermo quadrupole mass-spectrometer. The signals due to water (*m/z* = 18), H<sub>2</sub> (*m/z* = 2), N (*m/z* = 14), CO and N<sub>2</sub> (*m/z* = 28), P (*m/z* = 31), O<sub>2</sub> (*m/z* = 32), PH<sub>3</sub> (*m/z* = 34), CO<sub>2</sub> (*m/z* = 44), and P<sub>2</sub> (*m/z* = 62) were recorded during TPR.

Total acidity of the catalysts was determined by NH<sub>3</sub>-TPD technique using 150 mg of sample. Prior to the measurements, the samples were treated in situ with pure hydrogen (60 mL min<sup>-1</sup>) at 450 °C. The heating rate was 5 °C min<sup>-1</sup> and the final temperature was kept for 2 h. The system was then purged with He (30 mL min<sup>-1</sup>) for 30 min and then the sample was cooled down to 100 °C. The feed composition was switched to a mixture containing 5% NH<sub>3</sub> in He (30 mL min<sup>-1</sup>) for 30 min. Afterwards, the physisorbed ammonia was flushed out with flowing He (30 mL min<sup>-1</sup>) for 1 h. Desorption was measured under a heating rate of 10 °C min<sup>-1</sup> under He up to 600 °C. The reactor effluent was continuously monitored by quadrupole mass spectrometry (Pfeiffer Vacuum model).

CO chemisorption was performed at 30 °C to estimate the number of active sites in order to calculate TOF values. The solids containing either nickel oxide or the oxidic precursors of nickel phosphide (100 mg) were heated at 200 °C under helium (30 mL min<sup>-1</sup>) for 30 min and cooled down to 50 °C. Then, all solids have undergone treatment under the same conditions, i.e. under pure hydrogen (60 mL min<sup>-1</sup>) at 700 °C (heating rate 5 °C min<sup>-1</sup>), in order to obtain either Ni metallic phase or Ni<sub>2</sub>P phase from samples containing nickel oxide or Ni<sub>x</sub>P<sub>y</sub>O<sub>z</sub> precursors. XRD analysis confirmed that the expected phases were obtained after such treatment. The reactor was then cooled down to the adsorption temperature (30 °C) under helium (30 mL min<sup>-1</sup>). Successive pulses of pure CO (0.25 mL) were injected every 2 min. Results were collected by a gas phase chromatograph equipped with a TCD detector and a Porapak Q column (used to verify the absence of formation of CO<sub>2</sub> from CO) allowing the determination of the CO uptake value.

### 2.3. Activity measurements

A vertical continuous fixed-bed reactor (length: 40 cm; inner diameter: 1.26 cm) was used to study the transformation of m-cresol at 340 °C under 4 MPa. The pelletized catalysts (250–315 µm) diluted with silicon carbide (inert material) were placed in the reactor between two layers of quartz wool with layers of glass beads

on the top and the bottom. Prior to reaction, all catalysts were treated in-situ at 450 °C under 4 MPa for 2 h using pure hydrogen (4.7 NL h<sup>-1</sup>). A liquid model feed was prepared to obtain 53 kPa oxygenated reactant, 31 kPa n-heptane as internal standard and dodecane as solvent. The top inlet of the reactor was continuously fed by the liquid model feed using a HPLC Gilson pump and H<sub>2</sub> flow with a ratio hydrogen to oxygenate molar ratio of 486 NLL<sup>-1</sup>. In the reaction conditions, the H<sub>2</sub> partial pressure was set to 3.24 MPa.

Liquid samples were collected hourly from a condenser (Minichiller-Huber cryostat set to 10 °C located in the outlet line of the reactor). The samples were analyzed by a Varian 430 chromatograph with a DB1 capillary column (length: 30 m, inside diameter: 0.320 mm, film thickness: 5 µm) equipped with a flame ionization detector (FID). All products were identified by using a 1200 TQ mass spectrometer coupled with a Varian 3800 chromatograph and by co-injection of commercial compounds.

For each catalyst, experiments lasted 20 h on stream. During a single experiment set, the liquid inlet flow was varied to obtain different levels of conversion, keeping the ratio H<sub>2</sub>/oxygenate constant. The ratio between the catalyst weight and the oxygenated model compounds can be defined as space time ( $\tau$ , g h mol<sup>-1</sup>) in Eq. (1):

$$\tau = \frac{w}{F_{CRE}} \quad (1)$$

The reactant conversion of oxygenate ( $X_{CRE}$ , %) was calculated according to Eq. (2):

$$X_{CRE} = \frac{C_{CRE,0} - C_{CRE}}{C_{CRE,0}} \cdot 100 \quad (2)$$

$C_{CRE,0}$  being the initial molar fraction of m-cresol and  $C_{CRE}$  as the molar fraction of the corresponding reactant in the liquid sample collected at the studied space time  $\tau$ .

The selectivity of a product *i* ( $S_i$ , mol%) was given by Eq. (3):

$$S_i = \frac{C_i}{C_{CRE,0} - C_{CRE}} \cdot 100 \quad (3)$$

where  $C_i$  represents the molar fraction of a product *i* in the liquid sample analyzed.

Assuming a pseudo-first-order model, the global activity of catalyst ( $k_{Tot}$ , mmol h<sup>-1</sup> g<sup>-1</sup>) and the turnover frequency (TOF, in h<sup>-1</sup>) values can be estimated using Eqs. (4) and (5), respectively:

$$-\ln(1 - X_{CRE}) = k_{Tot} \cdot \tau \quad (4)$$

$$TOF = k_{TOT} / M \quad (5)$$

where  $M$  is the CO uptake (in mmol g<sup>-1</sup>) obtained from chemisorption measurement.

For all experiments, the mass balances were always between 95 and 100%. The reaction was carried out in the absence of internal and external mass-transfer effect as previously demonstrated [27].

## 3. Results and discussion

### 3.1. Catalyst characterization

**Table 1** lists the Ni and P loading of the samples obtained by ICP analysis. The Ni loading was around 9 wt.%. The Ni<sub>2</sub>P/SiO<sub>2</sub> and Ni<sub>2</sub>P/ZrO<sub>2</sub> samples showed a P/Ni molar ratio very close to the nominal values, being equal to 0.8 and 2.8, respectively. The adsorption-desorption isotherms of supports and catalysts before and after pretreatment step (450 °C, 4 MPa) are shown in Fig. S1 (Supplementary Information). According to the IUPAC classification, all the materials showed IV-type isotherm profiles, which were practically not affected by the nature of the active phase (Ni vs Ni<sub>2</sub>P). However, the type of hystereses was different between

**Table 1**Chemical composition and textural properties of the fresh<sup>†</sup> and treated<sup>‡</sup> samples.

Solid	(wt.%)		Specific surface area ( $\text{m}^2 \text{g}^{-1}$ )		Pore volume <sup>a</sup> ( $\text{cm}^3 \text{g}^{-1}$ )		Mesoporous volume <sup>b</sup> ( $\text{cm}^3 \text{g}^{-1}$ )		Average pore diameter <sup>c</sup> (nm)	
	Ni	P	fresh	treated	fresh	treated	fresh	treated	fresh	treated
$\text{SiO}_2$	–	–	208	–	0.54	–	0.57	–	9	–
$\text{ZrO}_2$	–	–	142	–	0.20	–	0.21	–	6	–
$\text{Ni/SiO}_2$	9.7	–	183	176	0.31	0.27	0.39	0.28	8	8
$\text{Ni/ZrO}_2$	10.1	–	128	125	0.17	0.16	0.17	0.17	6	5
$\text{Ni}_2\text{P/SiO}_2$	9.0	3.9	176	172	0.33	0.27	0.40	0.34	8	7
$\text{Ni}_2\text{P/ZrO}_2$	7.4	10.8	103	98	0.11	0.10	0.11	0.11	5	5

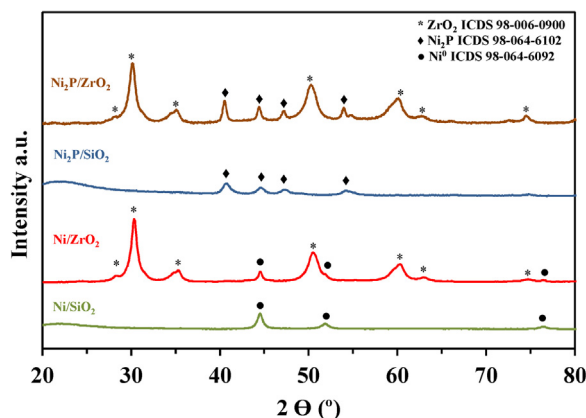
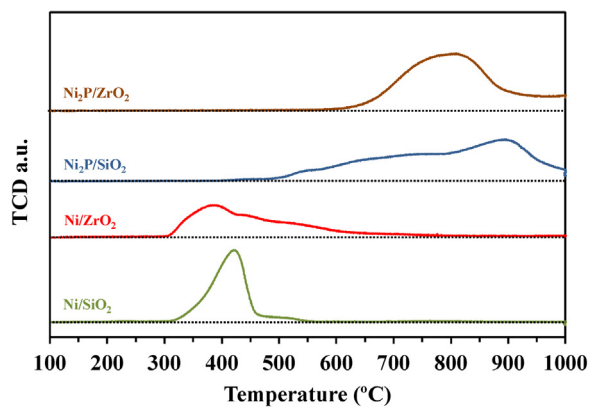
<sup>†</sup> fresh: dried and calcined samples.<sup>‡</sup> treated at 450 °C (5 °C min<sup>-1</sup>) under 4 MPa as total pressure during 2 h using pure H<sub>2</sub> (4.7 NL h<sup>-1</sup>).<sup>a</sup> calculated at P/P<sub>0</sub> equal to 0.98.<sup>b</sup> deduced from the t-plot method.<sup>c</sup> deduced from the BJH method using the adsorption branch.

Fig. 1. XRD patterns of nickel and nickel phosphide supported catalysts.

$\text{SiO}_2$  and  $\text{ZrO}_2$  materials. The hystereses loop of pure silica and silica supported catalysts was H2 type, characteristic of “ink-bottle” pore [38]. In contrast, the zirconia samples exhibited isotherms with type-H3 hystereses, which consist in aggregates of particles forming slit shaped nonuniform pores [38].

Table 1 summarizes the values of specific surface area, average pore volume and size for fresh and treated samples at 450 °C under 4 MPa of H<sub>2</sub>. Comparing the bare  $\text{SiO}_2$  and  $\text{ZrO}_2$  supports, the former exhibited higher specific surface area ( $208 \text{ m}^2 \text{ g}^{-1}$ ) and pore volume ( $0.57 \text{ cm}^3 \text{ g}^{-1}$ ) than the latter ( $142 \text{ m}^2 \text{ g}^{-1}$  and  $0.21 \text{ cm}^3 \text{ g}^{-1}$ , respectively). The addition of Ni and P decreased the specific surface area and pore volume that could be explained by a possible pore blocking. However, these properties were practically not affected by the pretreatment (450 °C, 4 MPa) allowing to obtain the desired phases ( $\text{Ni}^0$  or  $\text{Ni}_2\text{P}$ ).

The XRD patterns of all catalysts after the same pretreatment (450 °C, 4 MPa) and passivation procedure are shown in Fig. 1. Rietveld refinement of the diffractograms were performed to determine the crystallite size of the different catalysts with an isotropic model for the grain shape and for the microstrain. Excellent refinement of all the diffractograms were obtained (factor of goodness varying between 1.5 and 1.9) allowing a precise determination of the crystallite size (the uncertainty for the crystallite size is typically  $\pm 1 \text{ nm}$ ). The XRD pattern of  $\text{Ni/SiO}_2$  and  $\text{Ni/ZrO}_2$  catalysts exhibited the lines characteristic of  $\text{Ni}^0$  (ICDS 98-064-6090;  $2\theta = 45.5, 51.9$  and  $76.5^\circ$ ) and the lines corresponding to the respective supports; amorphous silica (a broad line between  $2\theta = 20$ – $30^\circ$ ) and tetragonal  $\text{ZrO}_2$  (main lines at  $2\theta = 30.2, 35.3, 50.5$  and  $60.2^\circ$ ) with an additional line at  $2\theta = 28.3^\circ$  (low intensity) corresponding to the presence of a monoclinic  $\text{ZrO}_2$  phase. The patterns of supported nickel phosphide catalysts showed that both silica and

Fig. 2. H<sub>2</sub>-TPR profiles of nickel and nickel phosphide supported catalysts. Conditions: 20 mL min<sup>-1</sup> 10% of H<sub>2</sub> in Ar with heating rate of 5 °C min<sup>-1</sup>.

zirconium were not altered by the addition of phosphorus. Both catalysts showed only the diffraction lines typical of the  $\text{Ni}_2\text{P}$  phase (ICDS 98-064-6102;  $2\theta = 40.6, 44.5, 47.3$  and  $54^\circ$ ). The diffraction lines corresponding to metallic Ni phase or oxyphosphates were not observed, demonstrating that the pretreatment used (450 °C, 4 MPa) allowed to obtain the desired nickel phosphide phase ( $\text{Ni}_2\text{P}$ ).

The particle size for all catalysts was calculated assuming uniform spherical particles (Table 2). These values were close to the values reported in the literature for the same type of catalyst [31,33,35]. The crystallite size depended on both the nature of the phase (Ni vs  $\text{Ni}_2\text{P}$ ) and the support used ( $\text{SiO}_2$  vs  $\text{ZrO}_2$ ). Metallic nickel and phosphide nickel particles were about 1.6–1.8 times higher when  $\text{ZrO}_2$  was used as support in comparison to  $\text{SiO}_2$  supported catalysts. Consequently, the dispersion of active phases was favored over silica, as already reported by several authors considering the  $\text{Ni}_2\text{P}$  phase [33,34]. This result is in agreement with the BET surface area of the supports (Table 1): the higher surface area of  $\text{SiO}_2$  ( $208 \text{ m}^2 \text{ g}^{-1}$ ) favored the formation of smaller particles compared to  $\text{ZrO}_2$  ( $142 \text{ m}^2 \text{ g}^{-1}$ ). Indeed, it was already reported that an increase in surface area of silica favored the dispersion of  $\text{Ni}_2\text{P}$  particles [39]. The nature of the support could also explain, at least in part, the difference in dispersion due to different metal/support interaction [40].

Fig. 2 shows the H<sub>2</sub>-TPR profiles of the calcined samples.  $\text{SiO}_2$  and  $\text{ZrO}_2$  supports did not exhibit any hydrogen consumption in the temperature range (100–1000 °C). The TPR profiles of nickel oxide supported over silica or zirconia revealed the same onset reduction temperature (300 °C). The presence of various peaks was observed on the TPR profile of  $\text{Ni/ZrO}_2$ , which exhibited a broad reduction region (between 300 and 600 °C). This seems to indicate that there are different  $\text{NiO}$  species that interact differently with  $\text{ZrO}_2$ : the

**Table 2**  
Catalysts properties.

Catalyst	H <sub>2</sub> uptake (mmol g <sup>-1</sup> )		d <sub>XRD</sub> <sup>d</sup> (nm)	NH <sub>3</sub> uptake <sup>e</sup> (μmol g <sup>-1</sup> )	CO uptake <sup>f</sup> (μmol g <sup>-1</sup> )
	Theoretical	Experimental <sup>c</sup>			
Ni/SiO <sub>2</sub>	1.5 <sup>a</sup>	1.6	10	0	21
Ni/ZrO <sub>2</sub>	1.6 <sup>a</sup>	1.7	17	179	33
Ni <sub>2</sub> P/SiO <sub>2</sub>	3.5 <sup>b</sup>	4.1	16	299	33
Ni <sub>2</sub> P/ZrO <sub>2</sub>	2.9 <sup>b</sup>	4.2	31	1020	38

<sup>a</sup> calculated to obtain Ni<sup>0</sup> calculated from Ni wt.% in the catalyst.

<sup>b</sup> calculated to obtain Ni<sub>2</sub>P calculated from Ni wt.% in the catalyst.

<sup>c</sup> determined by H<sub>2</sub>-TPR.

<sup>d</sup> particle size (d<sub>XRD</sub>) calculated from XRD.

<sup>e</sup> determined by TPD-NH<sub>3</sub>.

<sup>f</sup> determined by CO chemisorption.

weak metal/support interaction leading to peaks at lower temperature. In addition, distinct maximum uptakes were observed for both samples, at 386 °C for ZrO<sub>2</sub> and at 419 °C for SiO<sub>2</sub>. This shows that the reduction of some NiO particles were easier on ZrO<sub>2</sub>. The nickel oxide particles were completely reduced below 600 °C for both catalysts. The hydrogen consumption measured for both Ni/SiO<sub>2</sub> and Ni/ZrO<sub>2</sub> were very close to the theoretical values expected for the complete reduction of NiO to Ni<sup>0</sup>, as shown in Table 2. The fact that the desired Ni<sub>2</sub>P phase was obtained after the pre-treatment (as indicated in Fig. 1) was due to the use of a high pressure of hydrogen (4 MPa).

Nickel phosphide catalysts were prepared at higher temperatures than nickel oxide catalysts, which is in accordance with several studies [33,35,39]. These TPR profiles correspond to the preparation of the Ni<sub>2</sub>P phase from nickel oxyphosphate species (Ni<sub>x</sub>PyO<sub>z</sub>) [41]. Comparing the TPR profiles of Ni<sub>2</sub>P/SiO<sub>2</sub> and Ni<sub>2</sub>P/ZrO<sub>2</sub> catalysts, the H<sub>2</sub> consumption during the formation of the Ni<sub>2</sub>P phase supported over SiO<sub>2</sub> catalyst started at about 400 °C and was almost complete at 1000 °C. Several shoulders were observed, but the maximum H<sub>2</sub> consumption was achieved at 893 °C. For Ni<sub>2</sub>P/ZrO<sub>2</sub> catalyst, one large peak appeared at higher temperature compared to Ni<sub>2</sub>P/SiO<sub>2</sub> (between 588 and 950 °C), the maximum H<sub>2</sub> consumption being observed at about 795 °C.

The theoretical hydrogen consumption of each nickel phosphide catalyst, calculated considering the formation of Ni<sub>2</sub>P phase from the quantity of Ni present in the catalysts [27], is also reported in Table 2. Despite of the different P content, the H<sub>2</sub> consumption was approximately the same for both nickel phosphide catalysts (4.1–4.2 mmol g<sup>-1</sup>), which is 15% higher than the theoretical value for Ni<sub>2</sub>P/SiO<sub>2</sub> and 31% for Ni<sub>2</sub>P/ZrO<sub>2</sub>. The higher percentage for Ni<sub>2</sub>P/ZrO<sub>2</sub> can be explained by the high amount of P in the synthesis of this catalyst (P/Ni = 3) compared to Ni<sub>2</sub>P/SiO<sub>2</sub> (P/Ni = 0.8). In fact, the excess of hydrogen consumed is likely due to the formation of PH<sub>3</sub> species from phosphate species (such as PO<sub>4</sub><sup>3-</sup>, P<sub>2</sub>O<sub>7</sub><sup>2-</sup> or PO<sub>3</sub><sup>-</sup>) into PH<sub>3</sub> species [41]. Additional TPR experiments were performed to follow the phosphine (PH<sub>3</sub>–m/z = 34) signal during preparation of Ni<sub>2</sub>P/SiO<sub>2</sub> and Ni<sub>2</sub>P/ZrO<sub>2</sub> samples, which demonstrated the loss of P as PH<sub>3</sub> for both materials at high temperatures (Supplementary Information, Fig. S2).

The CO uptake measurement provides an estimation of the number of active sites of each phase (Ni(0) and Ni<sub>2</sub>P) [23,42]. These values reported in Table 1 are of the same order of magnitude of those reported in literature for similar loading of Ni-based catalysts [23,29].

NH<sub>3</sub>-TPD experiments were carried out to determine the strength and the density of the acid sites of the catalysts. The TPD profiles of the catalysts are shown in Fig. 3. Ni/SiO<sub>2</sub> did not show any peak, indicating that this catalyst has negligible acidity. Ni/ZrO<sub>2</sub> exhibited a broad peak at around 270 °C, which is attributed to the Lewis acidity due to Zr surface sites [40]. De Souza et al. [43] observed by DRIFTS of adsorbed pyridine that tetragonal zirconia

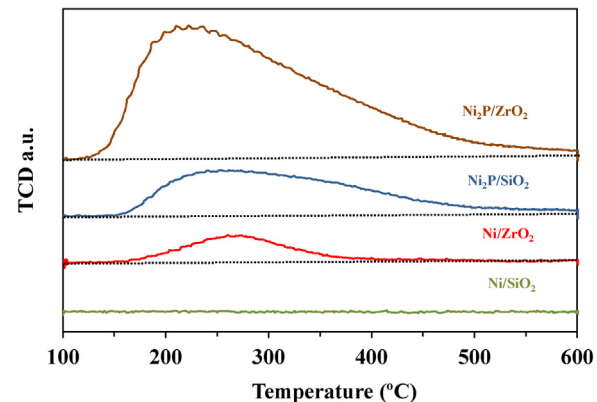


Fig. 3. NH<sub>3</sub>-TPD profile of Ni-based and Ni<sub>2</sub>P-based catalysts.

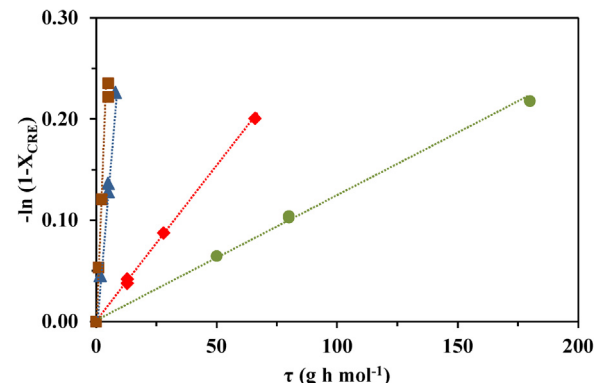


Fig. 4. Pseudo-first order plots of the HDO of m-cresol at 340 °C under 4 MPa; Ni/SiO<sub>2</sub> (●); Ni/ZrO<sub>2</sub> (◆); Ni<sub>2</sub>P/SiO<sub>2</sub> (▲); Ni<sub>2</sub>P/ZrO<sub>2</sub> (■).

revealed only the presence of Lewis acid sites. Comparing the NH<sub>3</sub>-TPD profile and the amount of desorbed ammonia for Ni<sub>2</sub>P and Ni supported catalysts, it is noticed that the presence of phosphorus increased significantly the density of acid sites, which is mainly due to the Brønsted acid sites attributed to the presence of PO–H groups formed on the support. The density of acid sites of all catalysts was also calculated from NH<sub>3</sub>-TPD profiles and the results are reported in Table 2. The density of acid sites followed the order: Ni<sub>2</sub>P/ZrO<sub>2</sub> > Ni<sub>2</sub>P/SiO<sub>2</sub> > Ni/ZrO<sub>2</sub> » Ni/SiO<sub>2</sub>.

### 3.2. Evaluation of Ni-based and Ni<sub>2</sub>P-based catalysts for the HDO of m-cresol

The hydrodeoxygenation of m-cresol was carried out under 4 MPa at 340 °C over Ni-based and Ni<sub>2</sub>P-based catalysts. Fig. 4 shows a linear relationship between –ln (1-X<sub>CRE</sub>) and τ for all

**Table 3**

Individual apparent rate constants determined during the transformation of m-cresol at 340 °C under 4 MPa of total pressure (standard deviation of rate constants close to 5%).

Catalyst	Rate constants (in mmol g <sup>-1</sup> h <sup>-1</sup> )							TOF (h <sup>-1</sup> )
	k <sub>Tot</sub>	k <sub>DOD</sub>	k <sub>HYD</sub>	k <sub>1</sub>	k <sub>2</sub>	k <sub>3</sub>	k <sub>4</sub>	
Ni/SiO <sub>2</sub>	1.13 ± 0.06	0.05 ± 0.01	1.08 ± 0.05	35 ± 2	3.0 ± 0.2	127 ± 6	–	54
Ni/ZrO <sub>2</sub>	3.00 ± 0.15	0.16 ± 0.01	2.84 ± 0.14	67 ± 3	108 ± 5	41 ± 3	32 ± 2	91
Ni <sub>2</sub> P/SiO <sub>2</sub>	28.3 ± 1.4	5.8 ± 0.3	22.5 ± 1.1	2254 ± 113	166 ± 8	552 ± 30	39 ± 3	570
Ni <sub>2</sub> P/ZrO <sub>2</sub>	47.0 ± 2.4	5.9 ± 0.3	41.0 ± 2.1	2385 ± 119	309 ± 15	835 ± 42	85 ± 4	1237

catalysts confirming that the overall reaction can be described as pseudo-first order (Eq. (4)), as previously proposed [27]. The calculated values of k<sub>Tot</sub> are given in Table 3 and follow the order: Ni<sub>2</sub>P/ZrO<sub>2</sub> > Ni<sub>2</sub>P/SiO<sub>2</sub> > Ni/ZrO<sub>2</sub> > Ni/SiO<sub>2</sub>. This trend shows that the Ni phosphide phase was much more active than the Ni metallic phase, irrespective the support used. The TOF values followed the same order as k<sub>Tot</sub>, in the range of 54 and 1237 h<sup>-1</sup>, clearly indicating that the intrinsic activity of an active site of nickel phosphide is much higher than the one of Ni. Nevertheless, studies reporting comparison of the HDO activity between Ni and Ni<sub>2</sub>P are still controversial. For example, Li et al. [23] showed that Ni/SiO<sub>2</sub> and Ni<sub>2</sub>P/SiO<sub>2</sub> exhibited approximately the same activity for the HDO of anisole at 300 °C under 1.5 MPa. The same result was obtained by Chen et al. [35] studying the HDO of methyl laurate under 2 MPa at 300 °C. On the contrary, Ni/SiO<sub>2</sub> was found 2.3 times more active than Ni<sub>2</sub>P/SiO<sub>2</sub> for the HDO of guaiacol at 350 °C under a lower pressure (0.5 MPa) [36]. It was demonstrated that an increase of pressure was more benefit for Ni<sub>2</sub>P than for Ni for HDO of methyl oleate [44]. Indeed, the authors reported that Ni/SBA-15 was 3.5 times more active than Ni<sub>2</sub>P/SBA-15 under 0.3 MPa, whereas both catalysts practically showed the same activity under 4 MPa. In our case, Ni<sub>2</sub>P clearly exhibited much higher activity than Ni, which can be in part related to the high pressure used in the present study (4 MPa).

The use of ZrO<sub>2</sub> as support increased the activity of both Ni and Ni<sub>2</sub>P based catalysts compared to SiO<sub>2</sub>. Regarding the influence of the support, the same result was observed by de Souza et al. [45] for the HDO of m-cresol at 300 °C under atmospheric pressure over SiO<sub>2</sub> and ZrO<sub>2</sub> supported Pd catalysts. The authors attributed this result to the presence of oxophilic sites represented by Zr<sup>4+</sup>/Zr<sup>3+</sup> cations near the periphery of metal particles. The oxophilic sites reduces the energy barrier for C–O bond cleavage, which is due to a strong interaction between the oxygen from the phenolic compound and the Zr cations. Our experimental results confirm that the oxophilicity of ZrO<sub>2</sub> plays a beneficial role for the HDO of phenolic compounds. Recently, it has been proposed in the literature that oxophilic sites (represented by unreduced metals and metal oxide cations from the supports) promote the deoxygenation pathway for HDO of different model molecules [18,45–48]. According to these studies, the strong bond between the oxygen from the phenol molecule and the oxophilic site might favor the hydrogenation of the carbonyl function or even the direct cleavage of the C–O bond. Some of these works performed DFT calculations to study the most energetically favorable reaction pathway. Some of us used DRIFTS of adsorbed cyclohexanone to measure the strength of the interaction between the oxygen of phenolic compounds and the oxophilic sites [49]. The results obtained revealed that more oxophilic cation such as Zr promotes the deoxygenation of phenol whereas the silica supported catalysts favored the hydrogenation of the aromatic ring. In addition, it should be emphasized that the textural properties of both supports used (SiO<sub>2</sub> and ZrO<sub>2</sub>) were quite different, and, obviously, leading to different textural properties between the catalysts. Nevertheless, based only on the catalytic results obtained, it is difficult to estimate the influence of the pore structure on the catalytic properties of the solids. Such information requires further

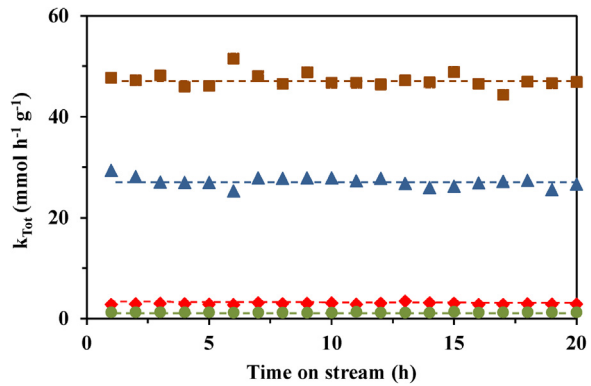


Fig. 5. k<sub>Tot</sub> as function of time on stream for the HDO of m-cresol at 340 °C under 4 MPa. Ni/SiO<sub>2</sub> (●); Ni/ZrO<sub>2</sub> (◆); Ni<sub>2</sub>P/SiO<sub>2</sub> (▲); Ni<sub>2</sub>P/ZrO<sub>2</sub> (■).

investigation by using, for example, several samples of ZrO<sub>2</sub> having different textural properties.

In the present work, experiments were performed during 20 h on stream and space times were modified during the transformation of m-cresol to obtain different values of conversion. Regardless of the conversion obtained and the  $\tau$  used, by recalculating the global apparent constant (k<sub>Tot</sub>) using Eq. (4), it is observed that very close values are obtained for each hour of experiment and catalyst (Fig. 5). Consequently, all catalysts exhibited a very good stability at least during 20 h on stream, highlighting the beneficial use of high pressure, as previously reported [27]. On the contrary, Li et al. [23] observed a deactivation profile of both Ni/SiO<sub>2</sub> and Ni<sub>2</sub>P/SiO<sub>2</sub> by carrying out the HDO of anisole at a lower pressure (1.5 MPa) at 300 °C. Similarly, previous studies reported Ni-based [19,23] and Ni<sub>2</sub>P-based [31,33] catalysts tend to deactivate at low H<sub>2</sub> pressure.

To investigate the effect of the active phase and the support on the selectivity of catalysts, the product distribution determined at the same level of conversion (close to 20%) is given in Table 4. The transformation of m-cresol yielded 3-methylcyclohexanone (3-MCHnone) and 3-methylcyclohexanol (3-MCHols) as oxygenated products, toluene (Tol), methylcyclohexenes (MCHes), methylcyclohexane (MCH) and ethylcyclopentane (ECP) as deoxygenated products.

MCH was always the main product over all catalysts, its amount varying between 57 mol% for Ni/ZrO<sub>2</sub> to 74 mol% for Ni<sub>2</sub>P/ZrO<sub>2</sub>. Concerning the Ni-based catalysts, the deoxygenation products (Tol + MCH + MCHes) were favored over Ni/ZrO<sub>2</sub> compared to Ni/SiO<sub>2</sub>. The higher deoxygenation selectivity of zirconia supported catalyst is likely due to its higher oxophilicity. Zirconia also promoted the production of MCHes, their selectivity being about twice higher for Ni/ZrO<sub>2</sub> compared to Ni/SiO<sub>2</sub>. In addition, the composition of methylcyclohexene isomers was dependent on the Ni-based catalyst (Table 4). Over Ni/ZrO<sub>2</sub>, 1-methylcyclohexene was the main alkene isomer, which is not the case for Ni/SiO<sub>2</sub>. From a thermodynamic point of view, the percentage of this isomer is expected to be equal to 65 mol% at 340 °C [50], which is very close to the experimental value reported for Ni/ZrO<sub>2</sub> (Table 4). In turn, 3- and

**Table 4**

Product distribution obtained from the transformation of m-cresol at 340 °C under 4 MPa of total pressure (conversion close to 20%).

Catalyst	$\tau$ (g h mol <sup>-1</sup> )	Conversion (%)	Selectivity (mol%)					1-MCHe/ MCHes	
			Tol	3-MChone	3-MCHols	MCHes	MCH		
Ni/SiO <sub>2</sub>	180.0	19.6	4.0	6.6	12.6	13.2	63.6	0	18
Ni/ZrO <sub>2</sub>	66.0	18.2	5.3	5.0	4.2	27.7	56.8	1.0	61
Ni <sub>2</sub> P/SiO <sub>2</sub>	8.0	20.2	20.6	1.6	0.0	13.8	62.9	1.1	65
Ni <sub>2</sub> P/ZrO <sub>2</sub>	5.0	20.9	12.7	0.0	0.0	9.9	74.3	3.1	65

4-MCHes are expected from dehydration of 3-MCHols. However, 1-methylcyclohexene cannot be directly produced. Its formation can be explained by the double-bond migration due to the presence of acid sites, which occurs in a high extent for Ni/ZrO<sub>2</sub> (acidic catalyst) reaching MCHes thermodynamic equilibrium. The Ni/SiO<sub>2</sub> catalyst does not exhibit any acidity as demonstrated by NH<sub>3</sub>-TPD, which explains the low 1-MCHe/MCHes ratio compared to Ni/ZrO<sub>2</sub>. In the same way, it was demonstrated that ZrO<sub>2</sub> exhibited high activity for the dehydration of cyclohexanol to cyclohexene, which was also attributed to its high density of acid sites [43].

The selectivity into oxygenated products (3-MCHols and 3-MChnone) was lower over the nickel phosphide based catalysts compared to metallic catalysts. Indeed, at 20% of m-cresol conversion, no oxygenates were detected over Ni<sub>2</sub>P/ZrO<sub>2</sub> and a small amount of 3-MChone was observed over Ni<sub>2</sub>P/SiO<sub>2</sub>. Therefore, the nickel phosphide promoted the formation of deoxygenated products. These differences will be further discussed in this manuscript.

Similarly to Ni/ZrO<sub>2</sub>, the 1-MCHe/MCHes ratio for both Ni phosphide catalysts showed that the thermodynamic equilibrium of MCHes is also reached due to their acidic properties. The use of Ni<sub>2</sub>P catalysts increased the selectivity into toluene compared to Ni catalysts: its selectivity was close to 5 mol% over both Ni/SiO<sub>2</sub> and Ni/ZrO<sub>2</sub> and equal to 12.7 and 21.6 mol% over Ni<sub>2</sub>P/ZrO<sub>2</sub> and Ni<sub>2</sub>P/SiO<sub>2</sub>, respectively (Table 4).

The selectivity into Tol, oxygenates (3-MChnone and 3-MChol), MCHes, MCH as function of m-cresol conversion is shown in Fig. 6. Toluene and oxygenates appeared as primary products. Alkenes were observed as intermediates, being hydrogenated into MCH at higher conversions. Since the selectivity into toluene was constant over all catalysts with the increase of conversion, it is considered that this aromatic was unreactive under these experimental conditions. In order to verify such assumption, additional sets of experiments were performed replacing m-cresol for toluene for each catalyst, which showed no hydrogenation of the aromatic compound for all catalysts.

Considering the analysis of Fig. 6, a plausible network for the transformation of m-cresol over Ni metallic and Ni phosphide phases, recently proposed in [27], is depicted in Scheme 1. It is assumed that the transformation of such phenolic compound proceeds via two parallel pathways. Toluene can be directly produced by the cleavage of the C–O bond of m-cresol (DDO pathway) while hydrogenation, hydrogenolysis and dehydration reactions can take place, leading to the formation of oxygenates, alkenes and alkanes (HYD pathway). For the latter pathway, 3-MChnone is probably obtained by the hydrogenation of m-cresol aromatic ring, which can further lead to 3-MCHols. The alcohols can be either directly transformed into methylcyclohexane by hydrogenolysis or into 3- and 4-methylcyclohexene by dehydration, these alkenes can be isomerized into 1-methylcyclohexene. MCHes can be hydrogenated into MCH. The appearance of ECP is a result of isomerization of MCH which also occurs on acid sites.

In order to measure the rate of these different reactions involved over Ni-based and Ni<sub>2</sub>P-based catalysts, a kinetic modeling based on the proposed reaction network (Scheme 1) was performed using an integral method. The same kinetic model was also used recently to determine the kinetic constants involved in the transformation

of cresol isomers using Ni<sub>2</sub>P/SiO<sub>2</sub> as catalyst [27]. A proper equation can be written:

$$r_{Tot} = -\frac{dC_{CRE}}{d\tau} = kC_{CRE}^{\alpha}P_{H_2}^{\beta} \quad (6)$$

where  $r_{Tot}$  is the total rate of the transformation of cresols,  $k$  is the reaction rate constant,  $C_{CRE}$  the molar fraction of a given cresol,  $P_{H_2}$  the partial pressure of hydrogen,  $\tau$  the space time defined previously,  $\alpha$  the reaction order in the cresol isomer, and  $\beta$  the reaction order in H<sub>2</sub>.

As hydrogen was used in a large excess compared to cresols, the hydrogen partial pressure was assumed to be constant. In addition, a pseudo-first order behavior was used to describe HDO of m-cresol. Consequently, Eq. (6) can be simplified as follows:

$$r_{Tot} = -\frac{dC_{CRE}}{d\tau} = k_{Tot}C_{CRE} \quad (7)$$

where  $k_{Tot}$  is the global apparent constant.

Several differential equations related to the transformation of m-cresol then can be written. For a sake of simplicity, the concentrations of oxygenated compounds have been put together and named  $C_{Oxy}$ .

$$-\frac{dC_{CRE}}{d\tau} = (k_{DDO} + k_{HYD}) C_{CRE} \quad (8)$$

$$\frac{dC_{Tol}}{d\tau} = k_{DDO}C_{CRE} \quad (9)$$

$$\frac{dC_{Oxy}}{d\tau} = k_{HYD}C_{CRE} - k_1C_{Oxy} - k_2C_{Oxy} \quad (10)$$

$$\frac{dC_{MCHes}}{d\tau} = k_2C_{Oxy} - k_3C_{MCHes} \quad (11)$$

$$\frac{dC_{MCH}}{d\tau} = k_1C_{Oxy} + k_3C_{MCHes} - k_4C_{MCH} \quad (12)$$

$$\frac{dC_{ECP}}{d\tau} = k_4C_{MCH} \quad (13)$$

where  $k_{DDO}$ ,  $k_{HYD}$ ,  $k_1$ ,  $k_2$ ,  $k_3$ ,  $k_4$  are the intrinsic rate constants involved in the transformation of m-cresol.  $C_{Tol}$ ,  $C_{Oxy}$ ,  $C_{MCHes}$ ,  $C_{MCH}$  and  $C_{ECP}$  are the molar fraction of toluene, oxygenates, methylcyclohexenes, methylcyclohexane and ethylcyclopentane, respectively.

The system of equations above (Eqs. (8)–(13)) was solved applying Runge–Kutta 4th order numerical integration algorithm. The values are shown in Table 3. Data fitting was performed by minimizing the residual sum of squares (RSS, Eq. (14)) between the molar fraction of each product obtained experimentally and the calculated values.

$$RSS = \sum (C_{i,exp} - C_{i,cal})^2 \quad (14)$$

where  $C_{i,exp}$  and  $C_{i,cal}$  are the experimental and calculated molar fraction of a component  $i$ .

The results of modeling for all catalysts are shown in Fig. S3 (Supplementary Information). The kinetic values determined ( $k_{HDO}$ ,  $k_{DDO}$ ,  $k_{HYD}$ ,  $k_1$ ,  $k_2$ ,  $k_3$  and  $k_4$ ) are given in Table 3.

Concerning the metallic Ni-based catalysts, Table 3 shows that  $k_{DDO}$  and  $k_{HYD}$  were about 3-fold higher for Ni/ZrO<sub>2</sub> than for

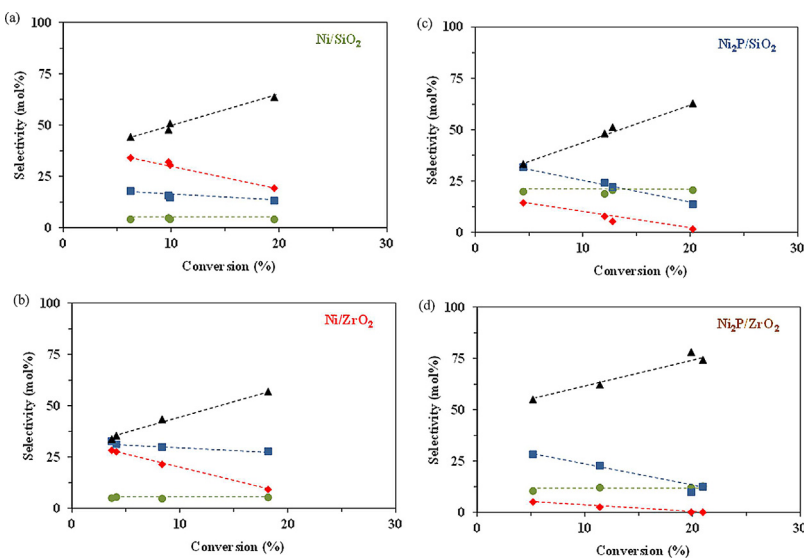
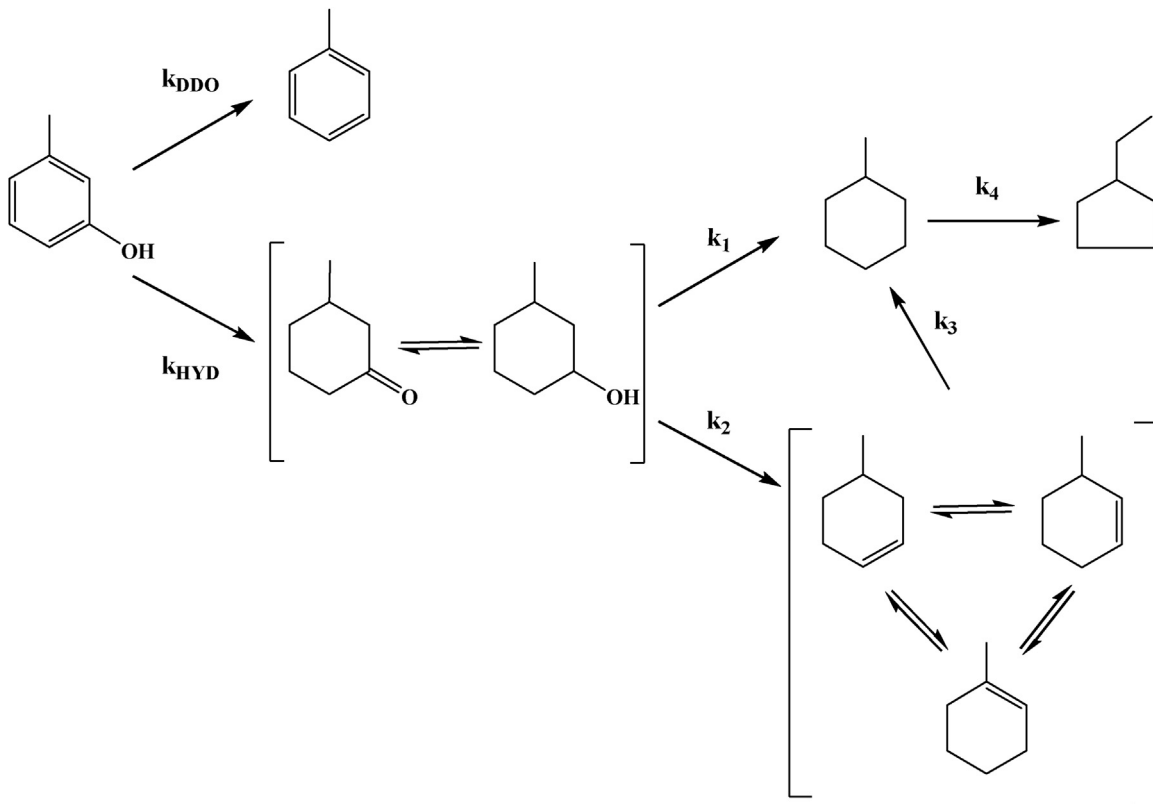


**Fig. 6.** Selectivity as function of conversion at 340 °C under 4 MPa. (▲) methylcyclohexane, (■) methylcyclohexenes; (◆) oxygenates (3-methylcyclohexanols and 3-methylcyclohexanone); (●) toluene; (—) Trend lines. (a) Ni/SiO<sub>2</sub>; (b) Ni/ZrO<sub>2</sub>; (c) Ni<sub>2</sub>P/SiO<sub>2</sub>; (d) Ni<sub>2</sub>P/ZrO<sub>2</sub>.



**Scheme 1.** Reaction network of the deoxygenation of m-cresol over Ni-based and Ni<sub>2</sub>P-based catalysts [27].

Ni/SiO<sub>2</sub>, highlighting the beneficial role of zirconia on the activation of oxygenated reactants, as already proposed in literature [14,22]. Indeed, the oxophilic sites present on zirconia can favor the adsorption of m-cresol through its oxygen atom on Zr cations, allowing the activation of the phenolic compound. In this case, hydrogen activated on metallic Ni particles participates on both hydrogenation and hydrogenolysis reactions. Such cooperative effect between metallic particles and ZrO<sub>2</sub> was already described to explain the HDO of phenol [14] and stearic acid [22]. A similar trend is observed for the transformation of 3-MCHols into MCH, k<sub>1</sub> value being two

times higher for Ni/ZrO<sub>2</sub> compared to Ni/SiO<sub>2</sub>. It can be assumed that the alcohol is also adsorbed on zirconia cations through its oxygen atom similarly as m-cresol. In the case of SiO<sub>2</sub>, weak acid sites (silanol groups) may not allow an activation of oxygenated compounds, explaining the lower activity of Ni/SiO<sub>2</sub>.

The rate of dehydration of alcohols was estimated by k<sub>2</sub> values. The irrelevant k<sub>2</sub> value of Ni/SiO<sub>2</sub> is in accordance with the fact that this catalyst does not exhibit any acidity, as observed by NH<sub>3</sub>-TPD (Fig. 4). On the contrary, the k<sub>2</sub> value was much higher over Ni/ZrO<sub>2</sub>, showing that the dehydration of alcohols was favored

over this catalyst due to the support acidity. As a consequence, the 3-methylcyclohexanol isomers were mainly deoxygenated by hydrogenolysis over Ni/SiO<sub>2</sub> and by dehydration over Ni/ZrO<sub>2</sub>. Indeed, the k<sub>1</sub>/k<sub>2</sub> ratio was high over the former (equal to 12) and low over the latter (equal to 0.6). As expected, the k<sub>4</sub> values measuring the isomerization of MCH into ECP (an acid-catalyzed reaction) followed the same trend than k<sub>2</sub>.

Among all kinetic values determined for nickel supported on SiO<sub>2</sub> and ZrO<sub>2</sub>, only the k<sub>3</sub> value was higher on Ni/SiO<sub>2</sub>. This result indicates that the hydrogenating properties related to the hydrogenation of alkenes into MCH was favored when SiO<sub>2</sub> was used as support. Actually, such observation may be explained by two main reasons: the difference in (i) particle sizes of nickel and/or (ii) the composition of alkenes mixture. Firstly, as the particles of Ni were smaller on SiO<sub>2</sub> (Table 2), it seems reasonable that the hydrogenation of alkenes is favored on Ni/SiO<sub>2</sub> compared to Ni/ZrO<sub>2</sub>, as proposed in literature [51]. Secondly, the alkenes mixture was mainly composed by 3- and 4-methylcyclohexenes over Ni/SiO<sub>2</sub> (Table 4). As these isomers present a higher reactivity in hydrogenation than 1-methylcyclohexene [52], this also justifies the higher value of k<sub>3</sub> determined over Ni/SiO<sub>2</sub>.

Irrespective to the support, it is clear that all kinetic constant values increased considerably when Ni<sub>2</sub>P-based catalysts were used instead of Ni-based catalysts (Table 3). Nevertheless, the influence of the support seems not to be the same for metallic and phosphide phases. As discussed above, the k<sub>DDO</sub> and k<sub>1</sub> values measure the rate of the C–O bond scission of m-cresol and methylcyclohexanols, respectively. These values were practically the same for Ni<sub>2</sub>P/SiO<sub>2</sub> and Ni<sub>2</sub>P/ZrO<sub>2</sub>, showing that hydrogenolysis reaction was not significantly affected by the nature of the support. On the contrary, the steps involving hydrogenation of either aromatic ring (k<sub>HYD</sub>) or double bond (k<sub>3</sub>) were higher on Ni<sub>2</sub>P/ZrO<sub>2</sub> than on Ni<sub>2</sub>P/SiO<sub>2</sub>. It can be noted that the increase of both k<sub>2</sub> (dehydration) and k<sub>4</sub> (isomerization) is in line with the modification of the acidic properties of catalyst (Fig. 4).

It is well known that the Ni<sub>2</sub>P phase is constituted by an orthorhombic crystalline structure that can present two different types of terminations along the (0001) direction, Ni<sub>3</sub>P and Ni<sub>3</sub>P<sub>2</sub> [30,42,53,54]. Recently, using cresol isomers as model molecules and Ni<sub>2</sub>P/SiO<sub>2</sub> as catalyst, we proposed that the Ni<sub>3</sub>P phase could be involved in the hydrogenation reactions and the Ni<sub>3</sub>P<sub>2</sub> in hydrogenolysis of C–O bond [27]. These proposals are in line with various studies reported in literature concerning HDO and HDS reactions [39,55,56]. It was proposed that cresol isomer can be adsorbed through their oxygen atom on three Ni neighbor atoms (hollow site), present on the Ni<sub>3</sub>P<sub>2</sub> termination, leading to C–O bond cleavage. Consequently, no effect of support is expected in this case, explaining why similar k<sub>DDO</sub> and k<sub>1</sub> values were obtained for Ni<sub>2</sub>P/SiO<sub>2</sub> and Ni<sub>2</sub>P/ZrO<sub>2</sub> (Table 3). Considering the HYD route, we have already suggested that the initial step requires a flat adsorption of m-cresol through its aromatic ring on the Ni<sub>3</sub>P termination allowing the complete hydrogenation of the aromatic ring leading to oxygenated intermediates (3-MCHnone and 3-MCHol) [27]. The fact that Ni<sub>2</sub>P/ZrO<sub>2</sub> presented a higher k<sub>HYD</sub> than Ni<sub>2</sub>P/SiO<sub>2</sub> might be attributed to a higher fraction of Ni<sub>3</sub>P termination that was favored by the zirconia support. As an evidence, further deep studies on catalyst structure using specific techniques such as PhotoEmission Electron Microscopy (PEEM) and Scanning Tunneling Microscopy (STM) are required, which could give more insights about the ratio Ni<sub>3</sub>P<sub>2</sub>/Ni<sub>3</sub>P for Ni<sub>2</sub>P supported catalysts. This kind of study was proposed by Suzuki et al. [57] and Moula et al. [58] but only over a single crystal Ni<sub>2</sub>P surface. In addition, as discussed above for Ni-based catalysts, ZrO<sub>2</sub> could also contribute indirectly by activating m-cresol through its oxygen atom on Zr cations favoring the HYD pathway.

## 4. Conclusion

The present study focused on the hydrodeoxygenation of m-cresol using both Ni and Ni<sub>2</sub>P active phases supported either on silica or zirconia. For all catalysts, m-cresol was deoxygenated through two parallel routes involving either C–O bond cleavage (Direct DeOxygenation route), or hydrogenation, dehydration, isomerization and hydrogenolysis steps (HYDrogenation route). The latter was always the major deoxygenation route and led mainly to methylcyclohexane. Toluene, the only DDO product, was more favored on Ni<sub>2</sub>P than on Ni, even though this deoxygenation route remained relatively low over all catalysts used. It was clearly demonstrated that the phosphide nickel phase (Ni<sub>2</sub>P) supported on zirconia exhibited the highest activity for m-cresol conversion. The reaction rate for the DDO pathway of both Ni<sub>2</sub>P catalysts was independent of the nature of support (silica or zirconia). However, the hydrogenation of the aromatic ring or the double bond as well as the dehydration and isomerization reactions were promoted on the zirconia supported Ni<sub>2</sub>P catalyst. The zirconia support could favor the presence of Ni<sub>3</sub>P terminations on the Ni<sub>2</sub>P/ZrO<sub>2</sub> and also the adsorption of m-cresol, enhancing the HYD activity. The highest dehydration and isomerization reaction rates are likely due to the higher density of Lewis (Zr cations) and Brønsted (P–OH groups) acid sites than silica.

## Acknowledgments

Vinicio O.O. Gonçalves and Priscilla M. de Souza thank the Conselho Nacional de Desenvolvimento Científico e Tecnológico (CNPq) for the scholarship. Fabio B. Noronha and Victor Teixeira da Silva acknowledge the financial support of the Conselho Nacional de Desenvolvimento Científico e Tecnológico (CNPq). Fabio B. Noronha is grateful to the University of Poitiers for the period as visiting professor.

## Appendix A. Supplementary data

Supplementary data associated with this article can be found, in the online version, at <http://dx.doi.org/10.1016/j.apcatb.2017.07.042>.

## References

- [1] T. Kan, V. Strezov, T.J. Evans, Lignocellulosic biomass pyrolysis: a review of product properties and effects of pyrolysis parameters, *Renew. Sustain. Energy Rev.* 57 (2016) 1126–1140.
- [2] D.C. Elliott, Biofuel from fast pyrolysis and catalytic hydrodeoxygenation, *Curr. Opin. Chem. Eng.* 9 (2015) 59–65.
- [3] C. Li, X. Zhao, A. Wang, G.W. Huber, T. Zhang, Catalytic transformation of lignin for the production of chemicals and fuels, *Chem. Rev.* 115 (2015) 11559–11624.
- [4] H. Shafaghat, P.S. Rezaei, W.M.A.W. Daud, Effective parameters on selective catalytic hydrodeoxygenation of phenolic compounds of pyrolysis bio-oil to high-value hydrocarbons, *RSC Adv.* 5 (2015) 103999–104042.
- [5] G. Yildiz, M. Pronk, M. Djokic, K.M. van Geem, F. Ronsse, R. Van Duren, W. Prins, Validation of a new set-up for continuous catalytic fast pyrolysis of biomass coupled with vapour phase upgrading, *J. Anal. Appl. Pyrolysis* 103 (2013) 343–351.
- [6] H. Prajirno, R. Insyani, J. Park, C. Ryu, J. Kim, Non-catalytic upgrading of fast pyrolysis bio-oil in supercritical ethanol and combustion behavior of the upgraded oil, *Appl. Energy*, 172 (2016) 12–22.
- [7] Y. Romero, F. Richard, S. Brunet, Hydrodeoxygenation of 2-ethylphenol as a model compound of bio-crude over sulfided Mo-based catalysts: promoting effect and reaction mechanism, *Appl. Catal. B Environ.* 98 (2010) 213–223.
- [8] V.O. Gonçalves, S. Brunet, F. Richard, Hydrodeoxygenation of cresols over Mo/Al<sub>2</sub>O<sub>3</sub> and CoMo/Al<sub>2</sub>O<sub>3</sub> sulfided catalysts, *Catal. Lett.* 146 (2016) 1562–1573.
- [9] O.I. Şenol, T.-R. Viljava, A.O.I. Krause, Effect of sulphiding agents on the hydrodeoxygenation of aliphatic esters on sulphided catalysts, *Appl. Catal. Gen.* 326 (2007) 236–244.

[10] S. Brilouet, E. Baltag, S. Brunet, F. Richard, Deoxygenation of decanoic acid and its main intermediates over unpromoted and promoted sulfided catalysts, *Appl. Catal. B Environ.* 148–149 (2014) 201–211.

[11] L. Nie, D.E. Resasco, Kinetics and mechanism of m-cresol hydrodeoxygenation on a Pt/SiO<sub>2</sub> catalyst, *J. Catal.* 317 (2014) 22–29.

[12] L. Wang, H. Wan, S. Jin, X. Chen, C. Li, C. Liang, Hydrodeoxygenation of dibenzofuran over SiO<sub>2</sub>, Al2O3/SiO<sub>2</sub> and ZrO<sub>2</sub>/SiO<sub>2</sub> supported Pt catalysts, *Catal. Sci. Technol.* 5 (2014) 465–474.

[13] P.M. de Souza, R.C. Rabelo-Neto, L.E.P. Borges, G. Jacobs, B.H. Davis, T. Sooknoi, D.E. Resasco, F.B. Noronha, Role of keto intermediates in the hydrodeoxygenation of phenol over Pd on oxophilic supports, *ACS Catal.* 5 (2015) 1318–1329.

[14] P.M. Mortensen, J.-D. Grunwaldt, P.A. Jensen, A.D. Jensen, Screening of catalysts for hydrodeoxygenation of phenol as a model compound for bio-oil, *ACS Catal.* 3 (2013) 1774–1785.

[15] C.A. Teles, R.C. Rabelo-Neto, J.R. de Lima, L.V. Mattos, D.E. Resasco, F.B. Noronha, The effect of metal type on hydrodeoxygenation of phenol over silica supported catalysts, *Catal. Lett.* 146 (2016) 1848–1857.

[16] X. Zhang, Q. Zhang, T. Wang, L. Ma, Y. Yu, L. Chen, Hydrodeoxygenation of lignin-derived phenolic compounds to hydrocarbons over Ni/SiO<sub>2</sub>–ZrO<sub>2</sub> catalysts, *Bioresour. Technol.* 134 (2013) 73–80.

[17] C. Zhao, Y. Yu, A. Jentys, J.A. Lercher, Understanding the impact of aluminum oxide binder on Ni/HZSM-5 for phenol hydrodeoxygenation, *Appl. Catal. B Environ.* 132–133 (2013) 282–292.

[18] L. Nie, P.M. de Souza, F.B. Noronha, W. An, T. Sooknoi, D.E. Resasco, Selective conversion of m-cresol to toluene over bimetallic Ni–Fe catalysts, *J. Mol. Catal. Chem.* 388–389 (2014) 47–55.

[19] X. Zhang, T. Wang, L. Ma, Q. Zhang, T. Jiang, Hydrotreatment of bio-oil over Ni-based catalyst, *Bioresour. Technol.* 127 (2013) 306–311.

[20] P.M. Mortensen, D. Gardini, H.W.P. de Carvalho, C.D. Damsgaard, J.-D. Grunwaldt, P.A. Jensen, J.B. Wagner, A.D. Jensen, Stability and resistance of nickel catalysts for hydrodeoxygenation: carbon deposition and effects of sulfur, potassium, and chlorine in the feed, *Catal. Sci. Technol.* 4 (2014) 3672–3686.

[21] S. Foraita, J.L. Fulton, Z.A. Chase, A. Vjunov, P. Xu, E. Baráth, D.M. Camaioni, C. Zhao, J.A. Lercher, Impact of the oxygen defects and the hydrogen concentration on the surface of tetragonal and monoclinic ZrO<sub>2</sub> on the reduction rates of stearic acid on Ni/ZrO<sub>2</sub>, *Chem. – Eur. J.* 21 (2015) 2423–2434.

[22] B. Peng, X. Yuan, C. Zhao, J.A. Lercher, Stabilizing catalytic pathways via redundancy: selective reduction of microalgae oil to alkanes, *J. Am. Chem. Soc.* 134 (2012) 9400–9405.

[23] K. Li, R. Wang, J. Chen, Hydrodeoxygenation of anisole over silica-supported Ni2P, MoP, and NiMoP catalysts, *Energy Fuels* 25 (2011) 854–863.

[24] H. Zhao, D. Li, P. Bui, S. Oyama, Hydrodeoxygenation of guaiacol as model compound for pyrolysis oil on transition metal phosphide hydropyrolysis catalysts, *Appl. Catal. Gen.* 391 (2011) 305–310.

[25] A. Berenguer, T. Sankaranarayanan, G. Gómez, I. Moreno, J. Coronado, P. Pizarro, D. Serrano, Evaluation of transition metal phosphides supported on ordered mesoporous materials as catalysts for phenol hydrodeoxygenation, *Green Chem.* 18 (2016) 1938–1951.

[26] S.T. Oyama, T. Onkawa, A. Takagaki, R. Kikuchi, S. Hosokai, Y. Suzuki, K.K. Bando, Production of phenol and cresol from guaiacol on nickel phosphide catalysts supported on acidic supports, *Top. Catal.* 58 (2015) 201–210.

[27] V.O. Gonçalves, P.M. de Souza, V.T. da Silva, F.B. Noronha, F. Richard, Kinetics of the hydrodeoxygenation of cresol isomers over Ni 2P/SiO<sub>2</sub>: proposals of nature of deoxygenation active sites based on an experimental study, *Appl. Catal. B Environ.* 205 (2017) 357–367.

[28] A. Infantes-Molina, E. Gralberg, J. Cecilia, E. Finocchio, E. Rodríguez-Castellón, Nickel and cobalt phosphides as effective catalysts for oxygen removal of dibenzofuran: role of contact time, hydrogen pressure and hydrogen/feed molar ratio, *Catal. Sci. Technol.* 5 (2015) 3403–3415.

[29] J.A. Cecilia, A. Infantes-Molina, E. Rodríguez-Castellón, A. Jiménez-López, S.T. Oyama, Oxygen-removal of dibenzofuran as a model compound in biomass derived bio-oil on nickel phosphide catalysts: role of phosphorus, *Appl. Catal. B Environ.* 136–137 (2013) 140–149.

[30] J.-S. Moon, E.-G. Kim, Y.-K. Lee, Active sites of Ni 2P/SiO<sub>2</sub> catalyst for hydrodeoxygenation of guaiacol: a joint XAFS and DFT study, *J. Catal.* 311 (2014) 144–152.

[31] S.-K. Wu, P.-C. Lai, Y.-C. Lin, Atmospheric hydrodeoxygenation of guaiacol over nickel phosphide catalysts: effect of phosphorus composition, *Catal. Lett.* 144 (2014) 878–889.

[32] H. Shi, J. Chen, Y. Yang, S. Tian, Catalytic deoxygenation of methyl laurate as a model compound to hydrocarbons on nickel phosphide catalysts: remarkable support effect, *Fuel Process. Technol.* 118 (2014) 161–170.

[33] S.-K. Wu, P.-C. Lai, Y.-C. Lin, H.-P. Wan, H.-T. Lee, Y.-H. Chang, Atmospheric hydrodeoxygenation of guaiacol over alumina-, zirconia-, and silica-supported nickel phosphide catalysts, *ACS Sustain. Chem. Eng.* 1 (2013) 349–358.

[34] J.-S. Moon, Y.-K. Lee, Support effects of Ni2P catalysts on the hydrodeoxygenation of guaiacol: in situ XAFS studies, *Top. Catal.* 58 (2015) 211–218.

[35] J. Chen, H. Shi, L. Li, K. Li, Deoxygenation of methyl laurate as a model compound to hydrocarbons on transition metal phosphide catalysts, *Appl. Catal. B Environ.* 144 (2014) 870–884.

[36] M.B. Griffin, F.G. Baddour, S.E. Habas, D.A. Ruddy, J.A. Schaidle, Evaluation of silica-supported metal and metal phosphide nanoparticle catalysts for the hydrodeoxygenation of guaiacol under ex situ catalytic fast pyrolysis conditions, *Top. Catal.* 59 (2015) 124–137.

[37] L. Lutterotti, S. Matthies, H. Wenk, MAUD: a friendly Java program for material analysis using diffraction, *IUCr Newslett. CPD* 21 (1999).

[38] G. Leofanti, M. Padovan, G. Tazzola, B. Venturelli, Surface area and pore texture of catalysts, *Catal. Today* 41 (1998) 207–219.

[39] S.T. Oyama, Y.-K. Lee, The active site of nickel phosphide catalysts for the hydrodesulfurization of 4,6-DMDBT, *J. Catal.* 258 (2008) 393–400.

[40] I. Rossetti, C. Biffi, C.L. Bianchi, V. Nichele, M. Signoretto, F. Menegazzo, E. Finocchio, G. Ramis, A. Di Michele, Ni/SiO<sub>2</sub> and Ni/ZrO<sub>2</sub> catalysts for the steam reforming of ethanol, *Appl. Catal. B Environ.* 117–118 (2012) 384–396.

[41] S. Oyama, X. Wang, Y.-K. Lee, K. Bando, F. Requejo, Effect of phosphorus content in nickel phosphide catalysts studied by XAFS and other techniques, *J. Catal.* 210 (2002) 207–217.

[42] R. Prins, M.E. Bussell, Metal phosphides: preparation, characterization and catalytic reactivity, *Catal. Lett.* 142 (2012) 1413–1436.

[43] P.M. de Souza, R.C. Rabelo-Neto, L.E. Borges, G. Jacobs, B.H. Davis, U.M. Graham, D.E. Resasco, F.B. Noronha, Effect of zirconia morphology on hydrodeoxygenation of phenol over Pd/ZrO<sub>2</sub>, *ACS Catal.* 5 (2015) 7385–7398.

[44] Y. Yang, C. Ochoa-Hernández, V.A. de la Peña O’Shea, J.M. Coronado, D.P. Serrano, Ni2P/SBA-15 as a hydrodeoxygenation catalyst with enhanced selectivity for the conversion of methyl oleate into n-octadecane, *ACS Catal.* 2 (2012) 592–598.

[45] P.M. de Souza, L. Nie, L.E. Borges, F.B. Noronha, D.E. Resasco, Role of oxophilic supports in the selective hydrodeoxygenation of m-cresol on Pd catalysts, *Catal. Lett.* 144 (2014) 2005–2011.

[46] M.B. Griffin, G.A. Ferguson, D.A. Ruddy, M.J. Biddy, G.T. Beckham, J.A. Schaidle, Role of the support and reaction conditions on the vapor-phase deoxygenation of m-cresol over Pt/C and Pt/TiO<sub>2</sub> catalysts, *ACS Catal.* (2016) 2715–2727.

[47] R.C. Nelson, B. Baek, P. Ruiz, B. Goundie, A. Brooks, M.C. Wheeler, B.G. Frederick, L.C. Grabow, R.N. Austin, Experimental and theoretical insights into the hydrogen-efficient direct hydrodeoxygenation mechanism of phenol over Ru/TiO<sub>2</sub>, *ACS Catal.* 5 (2015) 6509–6523.

[48] C. Newman, X. Zhou, B. Goundie, I.T. Ghompson, R.A. Pollock, Z. Ross, M.C. Wheeler, R.W. Meulenberg, R.N. Austin, B.G. Frederick, Effects of support identity and metal dispersion in supported ruthenium hydrodeoxygenation catalysts, *Appl. Catal. Gen.* 477 (2014) 64–74.

[49] P.M. de Souza, R.C. Rabelo-Neto, L.E.P. Borges, G. Jacobs, B.H. Davis, D.E. Resasco, F.B. Noronha, Hydrodeoxygenation of phenol over Pd catalysts. Effect of support on reaction mechanism and catalyst deactivation, *ACS Catal.* 7 (2017) 2058–2073.

[50] M. Peereboom, B. Van de Graaf, J. Baas, Experimental and calculated thermodynamic data for the isomeric methylcyclohexenes and methylenecyclohexane, *Recl. Trav. Chim. Pays-Bas* 101 (1982) 336–338.

[51] M. Che, C.O. Bennett, The influence of particle size on the catalytic properties of supported metals, *Adv. Catal.* 36 (1989) 55–172.

[52] R.A.W. Johnstone, J.-Y. Liu, L. Lu, D. Whittaker, Hydrogenation of alkenes over palladium and platinum metals supported on a variety of metal(IV) phosphates, *J. Mol. Catal. Chem.* 191 (2003) 289–294, [http://dx.doi.org/10.1016/S1381-1169\(02\)00212-1](http://dx.doi.org/10.1016/S1381-1169(02)00212-1).

[53] A.E. Nelson, M. Sun, A.S. Junaid, On the structure and composition of the phosphosulfide overlayer on Ni 2P at hydrotreating conditions, *J. Catal.* 241 (2006) 180–188.

[54] Q. Yuan, H. Ariga, K. Asakura, An investigation of Ni2P single crystal surfaces: structure, electronic state and reactivity, *Top. Catal.* 58 (2015) 194–200.

[55] H. Zhao, S.T. Oyama, H.-J. Freund, R. Włodarczyk, M. Sierka, Nature of active sites in Ni 2P hydrotreating catalysts as probed by iron substitution, *Appl. Catal. B Environ.* 164 (2015) 204–216.

[56] L.F. Feitosa, G. Berhault, D. Laurenti, T.E. Davies, V.T. da Silva, Synthesis and hydrodeoxygenation activity of Ni 2P/C-Effect of the palladium salt on lowering the nickel phosphide synthesis temperature, *J. Catal.* 340 (2016) 154–165.

[57] S. Suzuki, G.M. Moula, T. Miyamoto, Y. Nakagawa, K. Kinoshita, K. Asakura, S.T. Oyama, S. Otani, Scanning tunneling microscopy and photoemission electron microscopy studies on single crystal Ni2P surfaces, *J. Nanosci. Nanotechnol.* 9 (2009) 195–201.

[58] M.G. Moula, S. Suzuki, W.-J. Chun, S. Otani, S.T. Oyama, K. Asakura, The first atomic-scale observation of a Ni2P(0001) single crystal surface, *Chem. Lett.* 35 (2005) 90–91.